Synthesis and biological evaluation of 2.4 nm thiolate-protected gold nanoparticles conjugated to Cetuximab for targeting glioblastoma cancer cells via the EGFR

Nadja Groysbeck, Audrey Stoessel, Mariel Donzeau, Elisabete Cruz da Silva, Maxime Lehmann, Jean-Marc Strub, Sarah Cianferani, Kassiogé Dembélé, Guy Zuber

Synthesis and biological evaluation of 2.4 nm thiolate-protected gold nanoparticles conjugated to Cetuximab for targeting glioblastoma cancer cells *via* the EGFR

Nadja Groysbeck,[1] Audrey Stoessel,[1] Mariel Donzeau,[1] Elisabete Cruz da Silva,[2] Maxime Lehmann, [2] Jean-Marc Strub,[3] Sarah Cianferani,[3] Kassiogé Dembélé,[4] Guy Zuber[1]

1. Université de Strasbourg - CNRS, UMR 7242, Laboratoire de Biotechnologie et Signalisation Cellulaire, Boulevard Sébastien Brant, F-67400 Illkirch
2. Université de Strasbourg – CNRS, UMR 7021, Laboratoire de Bioimagerie et Pathologies, Faculté de Pharmacie F-67401 Illkirch
3. Université de Strasbourg - CNRS, IPHC UMR 7178, Laboratoire de Spectrométrie de Masse BioOrganique, F-67000 Strasbourg
4. Université de Strasbourg - Institut de Physique et Chimie des Matériaux de Strasbourg (IPCMS) 23 rue du Loess, F-67034 Strasbourg

E-mail: zuber@unistra.fr

Abstract

Therapeutic monoclonal antibodies benefit to patients and the conjugation to gold nanoparticles (AuNPs) might bring additional activities to these macromolecules. However, the behavior of the conjugate will largely depend on the bulkiness of the AuNP and small sizes are moreover preferable for diffusion. Water-soluble thiolate-protected AuNPs having diameters of 2 to 3 nm can be synthesized with narrow polydispersity and can selectively react with incoming organic thiols *via* a S_N2-like mechanism. We therefore synthesized a mixed thionitrobenzoic acid-, thioaminobenzoic acid- monolayered AuNP of 2.4 nm in diameter and developed a site-selective conjugation strategy to link the AuNP to Cetuximab, an anti-EGFR (Epidermal Growth Factor Receptor) antibody used in clinic. The water-soluble 80 kDa AuNP was fully characterized and then reacted to the hinge area of Cetuximab, which was selectively reduced using mild concentration of TCEP. The conjugation proceeded smoothly and could be analyzed by polyacrylamide gel electrophoresis, indicating the formation of a 1:1 AuNP-IgG conjugate as the main product. When added to EGFR expressing glioblastoma cells, the AuNP-Cetuximab conjugate selectively bound to the cell surface receptor, inhibited EGFR autophosphorylation and entered into endosomes like Cetuximab. Altogether, we describe a simple and robust protocol for a site-directed conjugation of a thiolate-protected AuNP to Cetuximab, which could be easily monitored, thereby allowing to assess the quality of the product formation. The conjugated 2.4 nm AuNP did not majorly affect the biological behavior of Cetuximab, but provided it with the electronic properties of the AuNP. This offers the ability to detect the tagged antibody and opens application for targeted cancer radiotherapy.

Key words: Gold nanoparticle, site-directed bioconjugation, antibody, targeted cancer therapy, epidermal growth factor receptor

Introduction

Nanoparticles (NPs) are particles of sizes ranging between 1 and 100 nm that have important biomedical applications [1]. Some NPs can be functionalized with multiple elements, which permits to provide the nanomaterial with new properties. The coalescence of several functions allows dealing with the complexity of biological systems and might help for diagnosing and treating diseases [2, 3]. Several sophisticated systems demonstrated some efficiencies at preclinical stages for imaging modalities [4], nucleic acid delivery [5], protein delivery [6], tissue-targeted drug delivery [7], hyperthermia and photoablation therapy [8]. Gold nanoparticles (AuNPs) have been extensively investigated for biomedical application, because they have a low toxicity profile and their unique optic and electronic properties can trigger cellular damage upon application of light [9] or radiation [10, 11]. Furthermore, AuNPs can be equipped with organic molecules, including antibodies, which facilitate accumulation of the AuNPs within selected tissues or cancer lesions [12]. AuNPs with diameters above 5 nm display a large surface area that can be used for tight adsorption of antibodies and other proteins [13, 14]. For example, El-Sayed *et al.* coated 40 nm AuNPs with monoclonal antibodies targeting the epidermal growth factor receptor (EGFR) by random adsorption in order to target oral squamous carcinoma cells. The antibody-mediated accumulation of these AuNPs into the cancer cells was then used to promote cell death *via* a photothermal treatment [9]. Patra *et al.* synthesized 5 nm AuNPs that were also surface-coated with anti-EGFR antibodies, as well as with gemcitabine for targeting the drug to cancer cells [15]. Although of straightforward practicability, the functionalization of AuNPs *via* adsorption to the particle's surface has limitations. Firstly, a control over the orientation and stoichiometry of the adsorbed molecules onto the AuNP is challenging [16]. Secondly, the physicochemical properties of the antibody and its subsequent cellular response are impacted by the AuNP's size [17, 18]. When the properties of an AuNP-IgG conjugate should resemble the ones of an antibody, AuNPs of smaller sizes should be selected. However, since antibodies do not tightly adsorb to the surface of small-sized AuNPs, the functionalization method must be adjusted by the formation of an Au-S coordination bond.

Small-sized and uniform AuNPs with diameters between 0.8 and 2 nm are easily prepared by reduction of chloroauric acid in the presence of organic thiols [19]. Thiobenzoate-protected AuNPs of such small sizes and of rather precise chemical composition can be directly prepared in aqueous solutions leading to water-soluble AuNPs. These AuNPs can be further grafted with biological macromolecules, such as oligonucleotides, peptides and proteins [20, 21], or viruses [22] by exchanging the thiobenzoate ligands with incoming thiol-containing macromolecules. To diminish unspecific association to cellular constituents and to enhance the ligand exchange reaction, we have previously developed a mixed thionitrobenzoic acid (TNBA), thioaminobenzoic acid (TABA) protected-AuNP of 1.4 nm diameter that showed diffusion abilities inside living cells after grafting with bioactive peptides [23]. This type of AuNP appeared to be particularly suited for the site-directed conjugation to an IgG at the antibody's hinge region. The hinge region of an IgG connects the complement-activating Fc domain to the antigen-binding (Fab) domain and contains disulfide bonds that can be selectively reduced to liberate nucleophilic thiols. These liberated thiols can then react with electrophiles, thereby forming covalent bonds [24, 25]. Moreover, they can also exchange with the ligands of thiolate-

protected AuNPs [26]. When the antibody is tagged at the hinge area, the antibody functionality is generally untouched since the Fab and the Fc domain, which both are implicated in the IgG cellular action, remain unmodified [27]. It should be however mentioned that the thiol-specific conjugation of AuNPs [28] and thiolate-protected AuNPs [26] at the hinge area is not always easy to achieve, likely due to steric hindrance.

In the presented study, we first modified a synthetic protocol for making a TNBA-, TABA-protected AuNP of 2.4 nm. Secondly, we evaluated the ability of this AuNP to react with the thiols of reduced IgGs at the hinge region (AuNP synthesis scheme and bioconjugation strategy illustrated in Figure 1). As models, we selected the anti-EGFR antibody Cetuximab (Cmab) and the anti-VEGF (vascular endothelial growth factor) antibody Bevacizumab (Bmab). The direct ligand exchange proceeded seamlessly at near stoichiometric ratio and the AuNP-antibody link remained intact, even after addition of the CALNNG peptide in large excess, which served the purpose of exchanging the remaining reactive TNBA/TABA ligands with a passive CALNNG layer [29]. Thirdly, the ability of the AuNP-Cetuximab conjugate to bind to its cellular target was assayed using cell line models. Biological evaluation using living cells with or without cell surface EGFR demonstrated that the AuNP-Cetuximab conjugate behaved very similarly to Cetuximab, despite being tagged with a 2.4 nm AuNP.

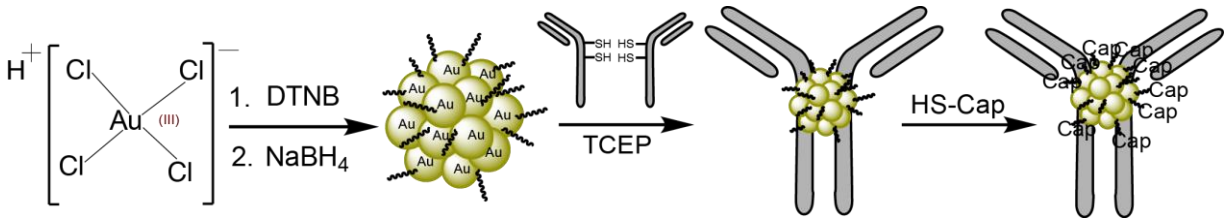

Figure 1. Scheme of gold nanoparticle (AuG) synthesis and bioconjugation to antibody. 1st step: Synthesis of AuG. Reduction of $HAuCl_4*3H_2O$ to organothiolate gold nanoparticle using $NaBH_4$ in the presence of DTNB (dithionitrobenzoic acid) in CH_3CN/H_2O (80:20) pH = 13. 2nd step: Thiolate-for-thiolate exchange of the selectively reduced antibody's hinge thiols and the AuG-ligands TNBA (thionitrobenzoic acid) and TABA (thioaminobenzoic acid). 3rd step: passivation of the AuNP-IgG conjugate using excess of peptide CALNNG (HS-Cap).

Materials and Methods

Chemicals

Water was purified with a Millipore Q-POD apparatus. The paraformaldehyde (PFA 16% solution) and the glutaraldehyde (25% solution) solutions were of Electron Microscopy quality grade and purchased from Electron Microscopy Sciences. The jet PRIME siRNA transfection reagent was from PolyPlus-transfection. Other chemical reagents and solvents were obtained from commercial sources (Sigma Aldrich, Carl Roth, Honeywell, VWR Chemicals) and used without further purification. The protein ladder for SDS-PAGE analysis was the Precision Plus Protein Standard Dual Xtra (BioRad). Peptides were purchased from GeneCust and the antibodies bevacizumab (Bmab) and cetuximab (Cmab) were provided by Centre de lutte contre le Cancer Paul Strauss (France) and originally purchased from Merck KGaA and Roche laboratory, respectively. The initial buffer solution of the antibodies Cmab and Bmab was changed to PBS

using illustra NAP-10 column (GE Healthcare). Antibodies used for the western blot analysis were purchased from Cell Signaling.

Materials

The pH of the solution was measured using a HI 2210 pH meter. Centrifugation of 50 mL tubes was performed with an Eppendorf 5810R centrifuge using an A-4-81 rotor. Centrifugation of smaller volumes (0.2 – 2 mL) was done using an Eppendorf 5415R centrifuge. A Heidolph Rotamax 120 rocking platform was used for mixing the gold reaction solution. Peptide coated AuNPs were purified and concentrated using Amicon Ultra 0.5 mL centrifugal filter devices (MWCO 10 kDa) if not stated otherwise. UV-Vis spectroscopy was performed on a Varian Cary 100Bio spectrometer.

Synthesis of the AuG gold nanoparticles

Solutions of 0.4 M $HAuCl_4*3H_2O$ (90 µL, 36 µmol) and 50 mM DTNB (5,5'-dithiobis-(2-nitrobenzoic acid), 1.08 mL, 54 µmol) in 0.3 M NaOH were added to 80:20 CH_3CN/H_2O mixture (10.8 mL) under stirring. The mixture was agitated for 6 h at room temperature before addition of a freshly prepared 0.75 M $NaBH_4$ solution in water (240 µL, 180 µmol). The orange colored solution immediately turned to black. After an overnight stirring, the precipitated AuNPs were recovered by centrifugation, washed with acetonitrile and then dried to yield the AuNP (named AuG) as a black powder.

Synthesis of AuNP-antibody conjugate

A 2 mg/mL antibody solution (225 µL, 0.45 mg) was treated with a 7 mM Tris(2-carboxyethyl)phosphine-HCl (TCEP) solution, pH 7.0 (90 µL, 0.63 µmol) for 1.5 h at 37°C. The AuG (73 µL of a 42 µM, 3.06 nmol) was then added to the reduced antibody (297 µL, 0.42 mg) in 0.1 M HEPES buffer, pH 7.5 at 25°C and the reaction was let to proceed overnight. The next day the AuNP-antibody conjugate was passivated with a 1 mM solution of peptide CALNNG (123 µL, 123 nmol or 40 molar eq. of AuNP-antibody conjugate) for 4 h at 25°C in 0.1 M HEPES buffer, pH 7.5. The exchanged AuG-ligands (TNBA and TABA) and excess CALNNG peptides were removed by ultrafiltration using Amicon 100 K ultracentrifugal devices.

Mass spectrometry analysis

Mass spectra were recorded with a MALDI-TOF MS operating in positive ion mode on an Autoflex™ system (Bruker Daltonics GmbH, Bremen, Germany). The system was used at an accelerating potential of 20 kDa in linear and reflector mode. The nitrogen laser (337 nm) was used at a frequency of 5 Hz and the acquisition mass range was set to 5000 – 30000 m/z with a matrix suppression deflection of 500 m/z. Samples were prepared by the dried droplet method. The matrix solution consisted of a saturated solution of α-cyano-4-hydroxycinnamic acid in H_2O/CH_3CN (50:50), which was threefold diluted in H_2O/CH_3CN/TFA (50:49.9:0.1).

Electron microscopy and EDX analysis

Images of the AuNPs were obtained by performing microscopy experiments using a C_s-corrected JEOL JEM-2100F Scanning Transmission Electron Microscope operating at 200 keV. Energy dispersive X-ray (EDX) analysis was carried out on the same instrument,

being equipped with an EDX detector. Samples were prepared by adding 10 µL of a 5 µM AuNP solution onto the Carbon film support of a ultrathin carbon 400 mesh Cu grid (Ted Pella Product No 01822-F, Redding, CA). After 2 min, excess liquid was blotted with a filter paper and the grid was dried for 48h.

FTIR analysis

Fourier-transform infrared (FTIR) spectrum of AuNPs was recorded using a Nicolet 380 FTIR spectrometer and a diamond ATR by Thermo Fisher Scientific (Supporting Information, Figure S1).

SDS-PAGE

SDS-PAGE was performed according to a published protocol of Laemmli *et al.* on 10% and 15% acrylamide gels [30]. The gels were pre-run for 20 min in a tris-glycine buffer (0.25 M Tris, 1.92 M glycine, 1%SDS, pH 8.5) at 20 mA. For loading 50% (v/v) glycerol solution was added to the AuNP solutions to a 5% final proportion. After electrophoresis, the AuNPs were seen as black-brown bands. Few amounts of AuNPs could be further visualized by silver enhancement. Proteins were revealed by Coomassie blue staining.

Cell culture

Cell lines were maintained in a 37°C humidified incubator with 5% CO_2. The human U87 glioblastoma cells (U87 MG, ATCC HTB-14) and the human fibrosarcoma cells (HT-1080, ATCC CCL-121) were maintained in Eagle's Minimum Essential Medium (EMEM) containing 10% fetal bovine serum (FBS), 1% sodium pyruvate and 1% nonessential amino acids. Human foreskin fibroblast (HFF) cells (HFF-1, ATCC SCRC-1041) were cultured in Dulbecco's Modified Eagle Medium (DMEM) supplemented with 2 mM L-glutamine, HEPES buffer, 10% heat inactivated fetal calf serum (FCS) and 50 µg/mL gentamycine. The U87 and HFF cells co-culture was done in Opti-MEM cell culture medium containing 10% FCS. The EGFR(+) U87 cell line was a gift from Professor Furnari [31]. The MTT assay was performed according to a published procedure [32].

Downregulation of EGFR expression in U87 cells

Expression of EGFR was down-regulated using the synthetic interfering RNAs (siRNAs) methodology. The U87 cell line was seeded in 6-well plates at 250 000 cells/well the day before the siRNA transfection experiment. For one well, a 50 nM siRNA solution (200 µL jetPrime buffer, 10 pmol siEGFR) was mixed with 4 µL of jetPrime reagent. After 10 min incubation at room temperature, the complexes were added to the cells by dilution into the cell culture medium. To ensure maximum gene silencing the cells were incubated for 48h before use [33]. The human EGFR siRNA solution (siGENOME Human EGFR(1956) siRNA Smart pool) was purchased from Dharmacon. The solution contained 4 siRNA molecules, which target the following mRNA sequences. Sequence 1: CCGCAAAUUCCGAGACGAA, sequence 2: CAAAGUGUGUAACGGAAUA, sequence 3: GUAACAAGCUCACG-CAGUU, sequence 4: GAGGAAAUAUGUACUACGA.

EGFR binding assay

Cells were seeded in 24-well plates and let to adhere on fibronectin-coated (20 µg/mL) glass coverslips the day before the assay. The cell culture medium was then replaced with a serum-free cell culture medium and the cells were incubated at 37°C for 30 min. This starvation step aimed at optimizing EGFR presentation on the cell surface [34]. Culture medium was then carefully removed and replaced with a serum-free medium containing the AuNP-antibody conjugate. After 30 min of incubation, the cell culture medium was removed. Cells were washed with PBS and then fixed with either 4% PFA in PBS (10 min) or 2.5% glutaraldehyde in Sorenson's Buffer (1h).

Assay of EGFR-mediated endocytosis

Cells were seeded in 24-well plates and let to adhere on fibronectin-coated (20 µg/mL) glass coverslips the day before the assay. The cell culture medium was then replaced with serum-depleted culture medium and the cells were let in this medium for 30 min at 37°C. After serum-depletion, cells were incubated in ice-cooled serum-free medium containing 167 nM of the AuNP-antibody conjugate. After 30 min of incubation on ice, the cell culture medium was replaced with pre-warmed serum-containing cell culture medium and the cells were incubated at 37°C for different time periods. The cell surface-bound antibodies were detached with a 0.2 M sodium acetate solution (pH 2.7). The cells were then washed with PBS and fixed with 4% PFA.

P**reparation of the cell specimen for AuNP detection**

The AuNPs were detected using a modified Danscher method [23, 35]. Briefly, after the 2.5% glutaraldehyde fixation step, the cells were incubated with a 0.1 M Sorenson's buffer, pH 7.4 containing 50 mM glycine for 20 min. The cell membrane was then permeabilized using a Sorenson's buffer, pH 7.4 containing 0.05% (w/v) saponine. The buffered solution was then replaced by a 0.1 M citrate solution, pH 6.7 containing 2% (w/v) sucrose. Development of the AuNPs was done in a dark room for 8 min using a freshly prepared 6 mM silver acetate solution in 0.16 M sodium citrate, pH 6.7 containing 2 mM propyl gallate and 20% (w/v) gum arabic. Development of the silver-mediated AuNP staining was stopped by washing the cell specimen with 0.16 M sodium citrate solution, pH 6.7.

Western blot

Cells were lysed in Laemmli loading buffer, the lysate was fractionated by SDS-PAGE and transferred onto a polyvinylidene difluoride (PVDF) membrane. The anti-EGFR D38B1, anti-pEGFR Tyr1068 and anti-GAPDH antibodies were used to detect EGFR, phosphorylated EGFR and GAPDH respectively.

Results

Gold nanoparticle synthesis and characterization

We previously described the synthesis of a TNBA-,TABA- protected AuNP of circa 102 gold atoms that could be grafted with thiolated peptides by exchanging most of the TNBA-ligands, leaving a surrounding zwitterionic protecting shell consisting of gold-coordinated TABAs [23].

In an initial stage, we explored the possibility of preparing the same type of TNBA-, TABA-protected AuNP, but of larger diameter. The nature and proportion of the solvents were seen to dramatically alter the production of thiolate-protected AuNPs [36]. We therefore assayed the reduction of $HAuCl_4$ with $NaBH_4$ and DTNB in various co-solvents. It was observed that a $HAuCl_4$/DTNB/$NaBH_4$ ratio of 1:1.5:5 in a solvent mixture of CH_3CN/H_2O (80:20) yielded to a AuNP population migrating as a discrete band when subjected to a sodium dodecyl sulfate polyacrylamide gel electrophoresis (SDS-PAGE) analysis, suggesting a homogenous population (Figure 2a).

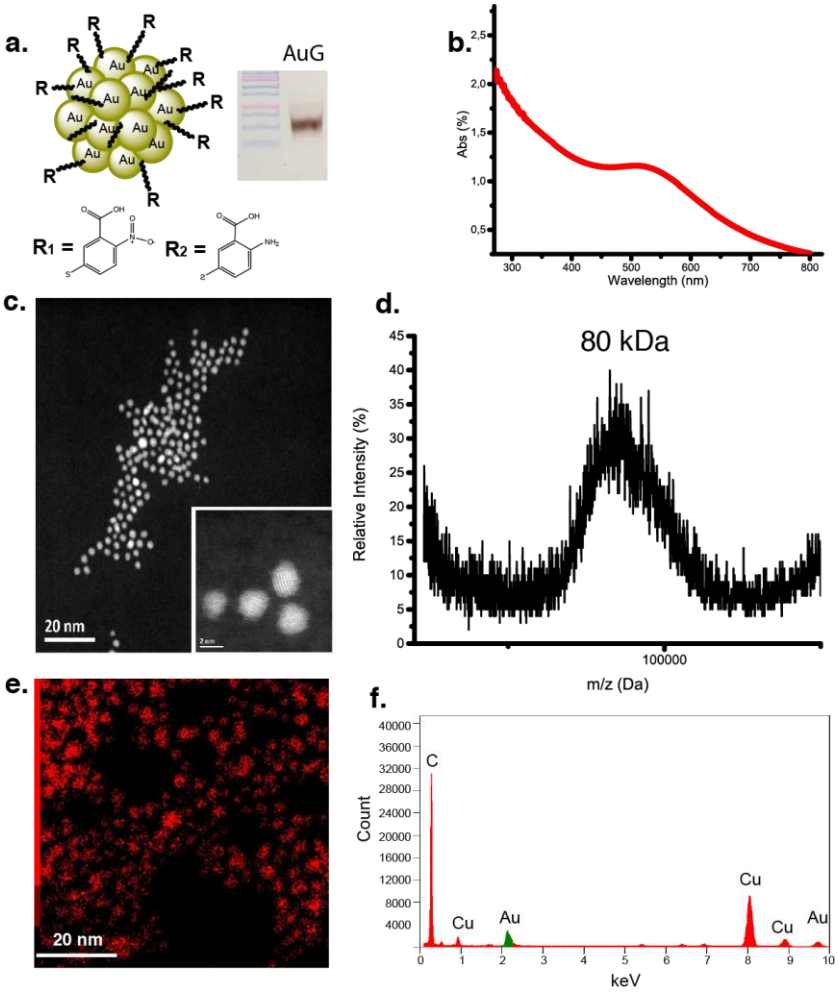

Figure 2. Characterization of 2.4 nm AuNP (AuG) **(a)** Structure and SDS-PAGE analysis of AuG (15% acrylamide gel). Structure of organothiolate ligands building the surface coating of AuG are depicted below the nanoparticle: R_1 = TNBA (thionitrobenzoic acid), R2 = TABA (thioaminobenzoic acid); **(b)** UV-Vis spectrum of AuG (small peak at 520 nm corresponding to weak surface plasmon resonance absorption); **(c)** Scanning transmission electron microscopy image of AuG particles. Inset image in right corner shows magnification (scale bar of main image: 20 nm, scale bar of inset image: 2 nm); **(d)** MALDI-TOF Mass spectrum of AuG (MW^{obs} = 80 kDa); **(e)** Elemental EDX mapping of AuG (scale bar: 20 nm); **(f)** EDX spectrum of AuG ($C_{K\alpha}$ = 0.277 keV, $Cu_{L\alpha}$ = 0.93 keV, $Au_{M\alpha}$ = 2.12 keV, $Cu_{K\alpha}$ = 8.04 keV, $Cu_{K\beta}$ = 8.9 keV, $Au_{L\alpha}$ = 9.71 eV).

This AuNP population (named AuG) was further characterized by UV-Vis spectroscopy (Figure 2b). Data showed that the absorption gradually increases for decreasing wavelengths. The spectrum contains a hump with a maximum absorption at 520 nm, corresponding to the weak surface plasmon resonance absorption of 2 nm diameter AuNPs [37]. The Scanning

Transmission Electron Microscopy (STEM) analysis of the AuNP revealed a homogenous population of spherical particles (Figure 2c) with a mean diameter of 2.4 ± 0.28 nm (n= 61). The observation of a crystalline lattice at high resolution (inset image in Figure 2c) confirmed that the metallic core of AuG was massive (Au^0). A MALDI-TOF mass spectrometry analysis of the AuNP (Figure 2d) displayed a narrow distribution of masses at 80 kDa, confirming the SDS-PAGE and EM data. By combining the different data and a volumetric density of 19.3 g/cm^3 for Au, we estimated that the AuNP contains on average about 420 gold atoms and 130 ligands. Further calculations and a test reaction using increasing ratios of a thiol-containing cationic peptide to the AuNP suggested that the ligand to peptide substitution saturates at about 35 exchanges per particle (Figure S2, Supporting Information). Energy Dispersive X-ray (EDX) analysis was also performed (Figures 2e and 2f). The spectrum displayed the characteristic peaks of gold ($Au_{M\alpha}$ at 2.12 keV; $Au_{L\alpha}$ at 9.712 eV) along with peaks corresponding to carbon and copper resulting from the carbon film-coated copper grid, on which the AuNPs were deposited for the analysis.

Conjugation to antibodies

The weakly nucleophilic and thiol-free reducing agent TCEP was used to reduce the antibody disulfide bridges [38]. For optimizing the reduction condition, the Cetuximab antibody (Cmab) was incubated with increasing TCEP concentrations and the reactions were monitored by SDS-PAGE analysis using non-reducing conditions (Supporting Information, Figure S3). Data showed that a final 2 mM TCEP concentration produced a complete reduction of the 150 kDa band to the expected 75 kDa band. Cmab was hence reduced with 2 mM TCEP in PBS for 90 min and the water-soluble 2.4 nm AuNP (AuG) was then directly added to the TCEP-reduced antibody mixture at a 1:1.2 (Cmab:AuNP) stoichiometry. The formation of the AuNP-Cetuximab conjugate (Au-Cmab) was monitored by SDS-PAGE using 10% acrylamide gels (Figure 3). To enable dual detection of the protein and the AuNP, the gel was firstly stained using Coomassie blue and then silver ions.

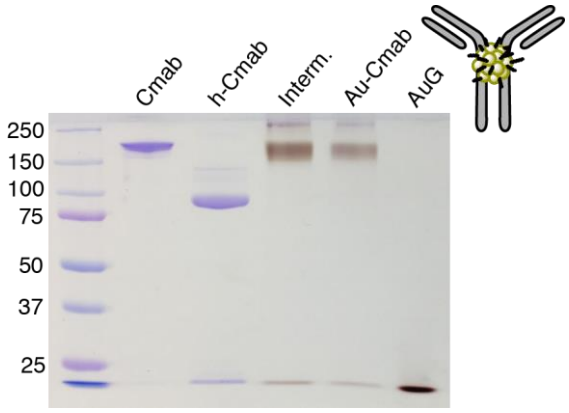

Figure 3. SDS-10% PAGE of gold nanoparticle-antibody-conjugate (Au-Cmab) formation under non-reducing conditions. Order on the gel from left to right: Cetuximab (Cmab), selectively reduced Cetuximab (h-Cmab), AuNP-Cetuximab conjugate before passivation (Interm.), AuNP-Cetuximab conjugate after passivation with peptide CALNNG (Au-Cmab), gold nanoparticle AuG

The conjugation reaction based on the substitution of an AuG ligand with a thiol group of the antibody's hinge area proceeded seamlessly, which could be concluded from the observation

of a black colored 150 kDa band and no remaining band at 75 kDa in the lane of Au-Cmab (Figure 3, lane 5). An apparent 250 kDa band was also observed suggesting dimerization of the IgG, but the proportion was estimated to be lower than 10%. We assumed that the major apparent 150 kDa band corresponds to a 1:1 AuNP-IgG conjugate, whereas the 250 kDa species possibly represents either a AuNP-$(IgG)_2$ product or an aggregate of two 1:1 AuNP-IgGs. The observation that the electrophoretic mobility of the main Au-Cmab conjugate was similar to the one of unreacted 150 kDa Cmab is puzzling. However, the AuNP migrated within the migration front and not as classical 80 kDa protein. This high electrophoretic mobility likely results from the high volumetric mass density of gold (19.3 g/cm^3) and the electronegative charge of AuG. A small amount of unreacted AuG was still detectable in the crude Au-Cmab solution (Figure 3, lane 5, faint band at the bottom of the gel), which likely resulted from the slight excess of AuG used for the reaction. Finally, the released ligands, as well as excess peptides and AuNPs were removed using a 100 kDa cut-off ultracentrifugation device. At the present stage, we were unable to remove all the AuNPs as judged by SDS-PAGE analysis, but obtained a batch with less than 5% of free AuNPs.

The conjugation of AuG to Bmab and the purification procedure were performed in a similar manner, but using a TCEP concentration of 0.1 mM for reduction of the hinge disulfide bonds (Supporting Information, Figure S4).

Biological evaluation of the Au-Cmab conjugate

The ability of the Au-Cmab to bind to EGFR, present on the surface of various cancer cells, was examined using a U87 glioblastoma cell line overexpressing the EGFR [31], hereafter referred to as EGFR(+) U87 cells. The Au-Bmab conjugate, which does not target the EGFR, but the vascular endothelial growth factor (VEGF), was used as the control. In a parallel control experiment, the EGFR expression of U87 wild type cells was almost abolished using the siRNA-mediated gene silencing technology to obtain EGFR(-) U87 cells (western blot confirming the successful downregulation of EGFR depicted in Figure S5, Supporting Information). The Cmab, Au-Cmab and Au-Bmab were added to living cells at a concentration of 167 nM by dilution into the cell culture medium. After 30 min of incubation, the cells were fixed and each domain of the conjugate was separately tracked (Figure 4). The antibody was detected by immunofluorescence (IF) [39] (Figure 4a). Green fluorescence (IgG) was only observed when Cmab and Au-Cmab were added to EGFR(+) U87 cells. Next, the AuNP moiety was revealed by gold-induced silver staining (Figure 4b). Analogous to the IF results, the strongest silver staining pattern was only seen for Au-Cmab-treated EGFR(+) U87 cells. Some silver staining was nonetheless observed within the endosomes of EGFR(-) and EGFR(+) cells for Au-Bmab and for Au-Cmab, suggesting that the AuNP domain somehow favors adherence to cell surfaces and subsequent endocytosis. It should be however mentioned that the silver-enhancement procedure is highly sensitive and not a quantitative method.

The ability of Au-Cmab to bind to EGFR-overexpressing cells was confirmed using an other EGFR-expressing cancer cell line (human fibrosarcoma cells, HT-1080; Supporting Information, Figure S6). As previously described for binding experiments using EGFR(+) U87 cells, the Au-Cmab bound to the surface of HT-1080 cells, whereas the control conjugate Au-Bmab did not show this pattern. Here again, we noticed some silver staining of the cells

incubated with Au-Bmab, reinforcing the assumption that the AuNP domain slightly promotes adherence to the cell surface and subsequent endocytosis.

These experiments convincingly demonstrated that Cmab and the Au-Cmab conjugate selectively bind to EGFR of living EGFR-presenting cells. We then evaluated the impact of the AuNP on the ability of Cmab to bind to the cell surface receptors. Cmab and Au-Cmab were incubated with the EGFR(+) U87 cells at concentrations ranging from 0.67 pM to 167 nM. The cells were fixed and the cell-attached antibodies were qualitatively detected by IF. An on/off fluorescence detection threshold was used and the on/off detection data were plotted as a function of the initial material concentration (Supporting Information, Figure S7). This rough quantitative analysis showed that the detection of the EGFR onto the cells required 10 times more of the Au-Cmab conjugate, than of Cmab, suggesting that appending the 2.4 nm AuNP at the hinge area may not be fully innocuous.

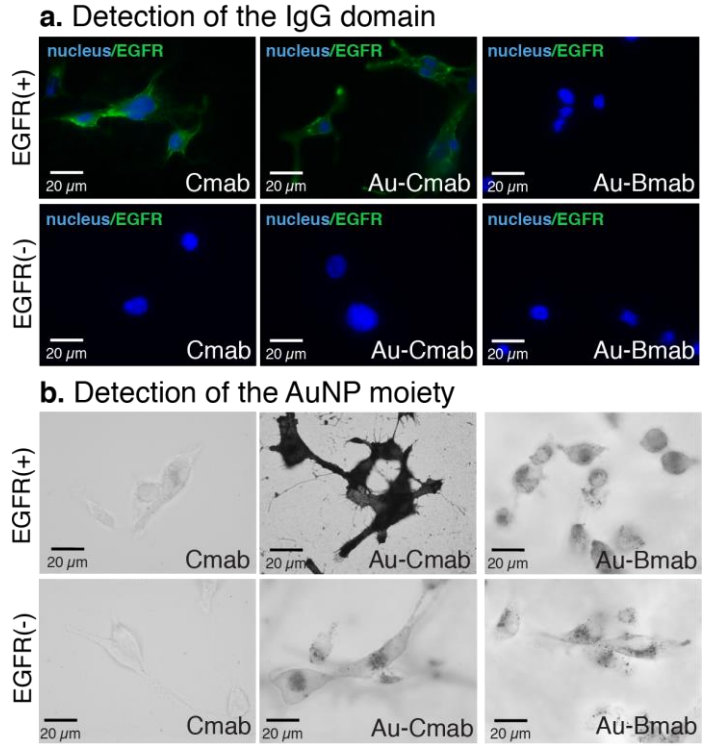

Figure 4. Analysis of the EGFR binding ability of the anti-EGFR Cmab, Au-Cmab and Au-Bmab to living EGFR(+) U87 glioblastoma cells and EGFR(-) U87 cells. **(a)** Detection of the antibody domain of the nanomaterial by immunofluorescence; **(b)** Detection of the AuNP domain by silver staining. Cells were incubated with 167 nM of antibody or AuNP-antibody conjugate for 30 min at 37°C. Scale bar: 20 µm

Next, we assayed the ability of the Au-Cmab to get internalized into cells, as it is described for Cmab [40]. Both compounds (Cmab and Au-Cmab) were incubated with living serum-starved EGFR(+) U87 cells for 30 min on ice to allow for receptor binding, but not for internalization. Afterwards, the sample- and non-serum-containing medium was exchanged for serum-containing cell culture medium and the cells were incubated at 37°C for 30 and 60 min, to allow internalization. At the end of the incubation, the nanomaterials bound to the cell surface receptors were washed away using a mild acidic treatment [41]. The cells were then fixed, the plasma membrane permeabilized with detergent, and the components detected by IF (Figure 5).

The time-course experiment showed that binding of Cmab and Au-Cmab to the cell surface receptors is followed by internalization into intracellular vesicular compartments. Although the intracellular fate of Cmab and Au-Cmab was similar, slight differences were observed at the 30 min incubation time-point. Cmab mainly localized into perinuclear compartments, whereas the Au-Cmab was still seen inside vesicles closer to the plasma membrane.

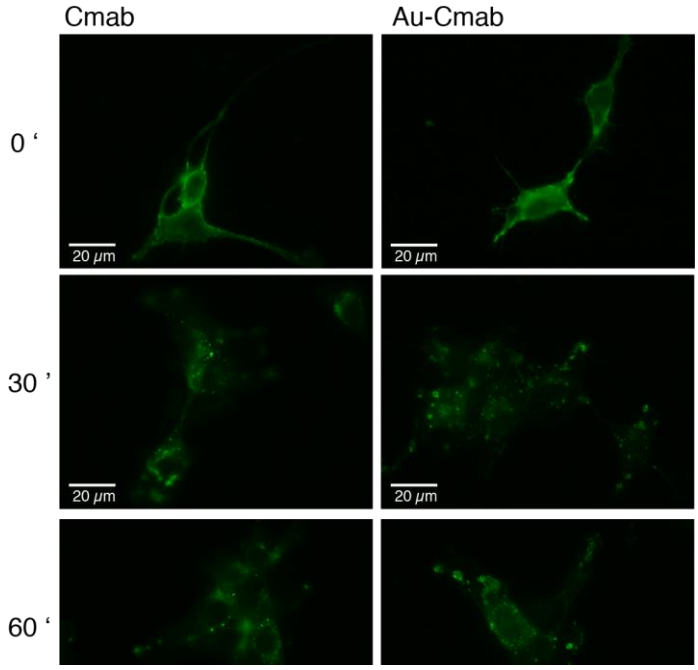

Figure 5. Assay of EGFR-mediated endocytosis. Cetuximab (Cmab) and AuNP-Cetuximab conjugate (Au-Cmab) were added to living EGFR(+) U87 cells for 30 min (37°C) at concentrations of 167 nM. The cell endocytosis was then evaluated immediately (image on top: 0’), as well as after 30 min and 60 min of further incubation in complete medium (not containing antibody and conjugate samples). The nanomaterial was detected by immunofluorescence. Scale bar: 20 µm

To further examine whether the biological function of Cmab was affected by the conjugation to AuG, we compared the ability of Cmab and Au-Cmab to inhibit EGFR autophosphorylation after induction with EGF. The serum-starved EGFR(+) U87 cells were incubated with Cmab and Au-Cmab together with EGF for 15 min at 37°C. Afterwards, the cells were lysed and the cell extracts were fractionated by SDS-PAGE to quantify the intracytosolic levels of EGFR and EGFR-pTyr1068 by western blot analysis (Figure 6). Data showed that the Au-Cmab inhibited the phosphorylation of EGFR similarly to Cmab [42].

Even though Cmab and the Au-Cmab inhibited EGFR phosphorylation, their addition to EGFR(+) U87 cells at a concentration of 167 nM did not apparently impact the cellular viability, as judged by a MTT assay (Supporting Information, Figure S8).

Finally, we examined whether the Au-Cmab conjugate is able to distinguish between EGFR-overexpressing cancer cells and non-cancerous cells. The EGFR(+) U87 cells were co-cultured with the non-cancerous human foreskin fibroblast (HFF) cells and the Au-Cmab was then added to the cell culture medium. After 30 min the cells were fixed and the presence of the Au-Cmab conjugate was revealed by IF and silver staining (Figure 7). The two cell types were easily distinguishable by their cell morphology. EGFR(+) U87 cells (Figure 7a: black arrows) are

much smaller and thinner than HFF cells (Figure 7a: red arrow; Figure 7b: cells encircled in red). Only the EGFR(+) U87 cells were engulfing a large proportion of Cmab and Au-Cmab, confirming that the Au-Cmab conjugate might be useful to selectively target EGFR-overexpressing tumor cells while not affecting non-cancerous cells.

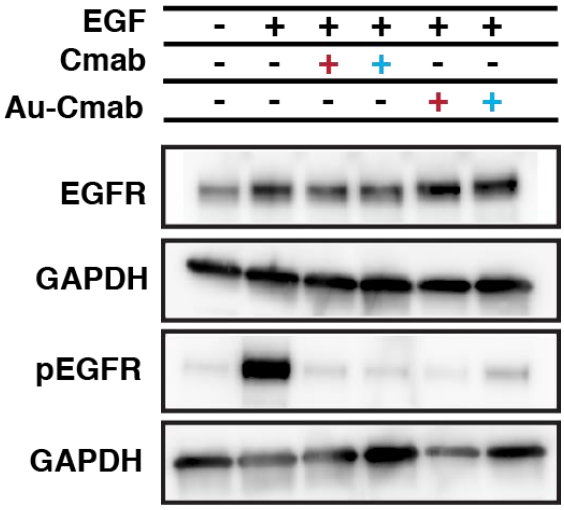

Figure 6. Western blot analysis of EGFR and phosphorylated EGFR (pEGFR) levels after addition of Cmab and Au-Cmab to EGF-stimulated EGFR(+) U87 cells. GAPDH was used as a loading control. Cmab and Au-Cmab were used at concentrations of 787 nM (left red +) and 394 nM (right blue +). EGF was used at a concentration of 8 nM.

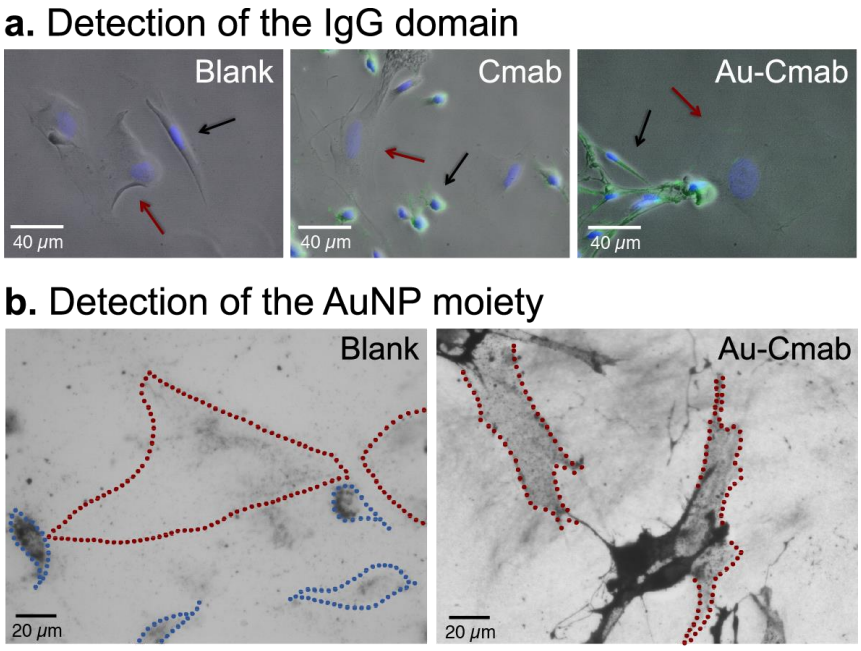

Figure 7. Evaluation of cell selectivity towards EGFR using a co-culture of EGFR(+) U87 cancer cells and non-cancerous human foreskin fibroblast (HFF) cells. Cmab or Au-Cmab were added to the co-culture by dilution in the cell culture medium. After 30 min incubation at 37°C the antibody domain and the AuNP moiety were detected by immunofluorescence **(a)** and silver staining **(b)**. The nuclei were stained in blue (DAPI). (**a)** HFF cells indicated by red arrow, EGFR(+) U87 cells indicated by black arrow. **(b)** HFF cells are encircled in red, EGFR(+) U87 cells are encircled in blue (in blank image only). Cmab and Au-Cmab concentrations used for incubation: 167 nM. Scale bar in **(a):** 40 µm, scale bar in **(b) :** 20 µm

Discussion

NPs, including AuNPs, can be prepared at various sizes and be equipped with functional organic components, which makes them useful for a multitude of different applications [43-48]. For biological applications, the AuNP size plays a major role. Particles having sizes above 4 – 5 nm offer the advantage to be easily detectable by electron microcopy and they can also be easily surface-coated with several antibodies using strong non-covalent binding or be coordination to organic molecules *via* an Au-S coordination [49, 50]. However, presentation of a large surface to macromolecules present in the solvent is not without consequence. When AuNPs are mixed with serum, a large protein corona is forming around the AuNPs [51] that can impact cellular interactions [52]. Beside these variations in physicochemical properties, the size plays an important role for the ADME (absorption, distribution, metabolism, excretion) profile of the particles [53-55]. Another parameter that is clearly impacting the ADME profile of NPs, such as elimination from the body, is the particle's coverage [56-58]. For inorganic non-biodegradable AuNPs, renal excretion should be undoubtedly favored, giving priority to the development of small AuNPs. Based on the work of Ackerson [59] we have prepared a novel type of AuNPs containing a mixed TABA, TNBA layer of circa 102 gold atoms that showed extremely promising usage for biological application, due to its abilities to be functionalized with peptides and to be stabilized with zwitterionic ligands [23]. Although we could have used this AuNP for conjugation, we wished to prepare slightly larger NPs for increasing the quantity of gold atoms within the system on the one side, but also to increase the conjugation challenge as bulkiness provides steric hindrance and unspecific interactions [60, 61]. While it is well described that increasing the NP size can increase the formation of protein corona [62], the size-threshold for the occurrence of protein corona for thiolate-protected AuNPs and the associated change in the particle's physicochemical properties, is unknown. To start answering to this question, we have hence privileged to work with AuNPs of 2.4 nm, instead of with AuNPs of 1.4 nm.

A previous investigation showed that mercaptobenzoic acid-protected AuNPs can be prepared at various sizes by adjusting the type and composition of the solvent mixture used for the particle synthesis [36]. In our case, a solvation of the gold-DTNB complex in an acetonitrile/water (80:20) mixture led to 2.4 nm AuNPs showing a high degree of monodispersity that could be characterized by SDS-PAGE analysis, MALDI-TOF mass spectrometry, STEM, EDX and UV-Vis spectroscopy.

The site-directed bioconjugation of the antibodies Cmab and Bmab to the AuG *via* simple thiolate-for-thiolate ligand exchange proceeded smoothly and could be monitored by non-reducing SDS-PAGE. Until today there are very few reports about the controlled conjugation of large biomolecules to small-sized AuNPs. Ackerson and coworkers attempted the "direct" labeling of cysteine-containing proteins with Au_{144}NPs, however the reaction seemed to require a large excess of NPs, as a large quantity of unreacted AuNPs could be detected on the SDS gels, indicating that the reaction did not proceed as straightforward as it was the case in the present study [26]. The following reason could be hypothesized. The AuNPs produced by Ackerson *et al.* were coated with mercaptobenzoic acid, while the particles of the present study contained zwitterionic thioaminobenzoate ligands. This zwitterionic coating might diminish unspecific associations between the nanoparticle and the biomolecule, thereby favoring the accessibility of the AuNP to the antibody's hinge thiols and consequently the S_N2-like substitution.

The ability of Au-Cmab to selectively bind to EGFR present on living cells was assayed using U87 glioblastoma cells that were engineered to overexpress the EGFR, as well as using the human HT-1080 fibrosarcoma cell line, which also overexpresses the EGFR. The glioblastoma cell model system was chosen, because 40% of all glioblastoma patients overexpress the EGFR, however the response to any EGFR-based therapeutic treatment is extremely low, an issue, which remains unresolved until today [63-65]. As a consequence approaches have been developed to use the anti-EGFR antibody Cmab as a cancer targeting agent to deliver active payloads [63]. These active payloads can hence induce cell damage of the targeted cells, without relying on a "normal functioning" EGFR signaling pathway. The data obtained from the EGFR binding assays of the present study showed that the Au-Cmab conjugate selectively binds to the EGFR on living cells in an analogous, but not identical manner than Cmab. The following AuNP-mediated differences were observed. First, an AuNP-mediated endocytosis was noted, suggesting that the 2.4 nm AuNPs slightly bind by themselves to cell surfaces. The association of the AuNP to the cell membrane was moreover promoting a small change in the intracellular trafficking of the Au-Cmab, confirming some AuNP-mediated non-selective associations to cell surface membranes. The relevance of this slight, but apparent difference between Cmab and AuCmab is unclear but deserves careful attention. Finally, the conjugation of the AuNP decreased the apparent binding affinity. However, it should be emphasized that we have not comprehensively optimized the quality of the Au-Cmab conjugate and the magnitude in decrease of binding affinity, which we have observed (10 times difference), might be reduced.

The cell viability of the EGFR(+) U87 cells was not diminished by incubation with Cmab or Au-Cmab. This absence of toxicity has already been reported for cultured glioblastoma cells [66] and we hypothesize that this issue has the same background as the resistance of glioblastoma tumors to EGFR-based therapies.

Altogether, we reported a synthesis of highly uniform 2.4 nm AuNPs that can be site-directly conjugated to the antibodies Cmab and Bmab *via* a straightforward thiolate-for-thiolate exchange mechanism. Data from *in vitro* studies showed that the Au-Cmab conjugate was able to specifically bind and internalize into glioblastoma cells after binding to EGFR, demonstrating that a targeted accumulation of AuNPs within cancerous cells is achievable. Since AuNPs allow for radiosensitization [67, 68], can be readily conjugated to drugs [69], or

can be prepared from β-emitting radioactive gold-189 [70, 71], the Au-Cmab conjugate holds promise for targeted anticancer therapy of glioblastoma tumors, which are resistant to traditional EGFR-based therapeutic treatments.
At the present stage of investigation and knowledge, antibodies and by extension "antibody-like" conjugates should circulate in the blood after intravenous injection. Assuming that, the pharmacokinetic properties of Au-Cmab are identical to the ones of Cmab, a blood half-life of 18 – 21 days can be expected with an elimination by intracellular catabolism [72], rather than by renal filtration or hepato-biliary mode [73]. This pharmacokinetic behavior should facilitate targeted accumulation of the conjugate at cancer lesions, but raises issues about the reminiscence of AuNPs inside the body after degradation of the antibody moiety. Although it is generally accepted that particles having a hydrodynamic diameter <6 nm are rapidly cleared from the body by renal filtration [73], the elimination of the 2.4 nm AuNPs need to be examined by *in vivo* studies. Moreover, *in vivo* experiments should be performed to study the route of administration, the biodistribution and the fate of the Au-Cmab conjugate.

Conclusion

A highly defined 2.4 nm AuNP, displaying an inner metallic core and an Au-S coordinated organic ligand shell, was synthesized by $NaBH_4$ reduction of chloroauric acid in the presence of the Ellman's reagent in a 80:20 acetonitrile/water mixture. This 2.4 nm AuNP could be characterized using several methods including MALDI-TOF mass spectrometry, SDS-PAGE, UV-Vis spectroscopy, electron microscopy, FTIR and EDX analysis, thereby facilitating the reproducibility of production. The AuNP was subsequently functionalized with the anti-EGFR antibody Cmab *via* a simple thiolate-for-thiolate exchange of the AuG ligands (TNBA and TABA) and the hinge thiols of the selectively reduced antibody – a site-directed conjugation strategy, which has not been explored before for antibodies and small-sized AuNPs. To minimize the formation of protein corona and to prevent NP aggregation, the Au-Cmab conjugate was passivated with peptide CALNNG in a second step. To demonstrate that the conjugation strategy is generally applicable, the AuNP was also conjugated to the VEGF-targeting antibody Bmab. Besides, the Au-Bmab conjugate served as control in the EGFR binding assays. The conjugation reactions could be readily visualized using non-reductive SDS-PAGE analysis, from which it was assessed that the major conjugation products consist of one IgG and one AuNP. The generated Au-Cmab conjugate was seen to behave similarly to Cmab when added to living cells, suggesting that the site-directed conjugation to the AuNP did not destroy the biological activity of the antibody, thereby demonstrating the value of the designed functionalization strategy. The possibility to produce very defined AuNP-IgG conjugates opens now new ways to assay the Au-Cmab conjugate for cancer therapy, either for sensitizing tumor cells to external radiation [10], or as a vehicle for the delivery of radioactive gold isotopes to tumor sites [70, 71, 74].

Acknowledgement

This research was supported by the ANR-10-LABX-0026_CSC and the French Proteomic Infrastructure (ProFI, ANR-10-INBS-08-03). N.G. received a Ph.D. fellowship from the IdEX Unistra (Université de Strasbourg and Investissements d'Avenir).

The authors and co-authors have no conflicts of interest.

References

1. McNamara, K. and S.A.M. Tofail 2016 Nanoparticles in biomedical applications. *Advances in Physics: X.* **2**(1) 54-88.
2. Ma, X., Y. Xiong, and L.T.O. Lee 2018 Application of Nanoparticles for Targeting G Protein-Coupled Receptors. *Int J Mol Sci.* **19**(7).
3. Muhamad, N., T. Plengsuriyakarn, and K. Na-Bangchang 2018 Application of active targeting nanoparticle delivery system for chemotherapeutic drugs and traditional/herbal medicines in cancer therapy: a systematic review. *Int J Nanomedicine.* **13** 3921-3935.
4. Tong, L., et al. 2009 Gold nanorods as contrast agents for biological imaging: optical properties, surface conjugation and photothermal effects. *Photochem Photobiol.* **85**(1) 21-32.
5. Zuber, G., M. Dontenwill, and J.P. Behr 2009 Synthetic viruslike particles for targeted gene delivery to alphavbeta3 integrin-presenting endothelial cells. *Mol Pharm.* **6**(5) 1544-52.
6. Chiper, M., K. Niederreither, and G. Zuber 2018 Transduction Methods for Cytosolic Delivery of Proteins and Bioconjugates into Living Cells. *Adv Healthc Mater.* **7**(6) e1701040.
7. Farooq, M.U., et al. 2018 Gold Nanoparticles-enabled Efficient Dual Delivery of Anticancer Therapeutics to HeLa Cells. *Sci Rep.* **8**(1) 2907.
8. Dykman, L. and N. Khlebtsov 2012 Gold nanoparticles in biomedical applications: recent advances and perspectives. *Chem Soc Rev.* **41**(6) 2256-82.
9. El-Sayed, I.H., X. Huang, and M.A. El-Sayed 2006 Selective laser photo-thermal therapy of epithelial carcinoma using anti-EGFR antibody conjugated gold nanoparticles. *Cancer Lett.* **239**(1) 129-35.
10. Hainfeld, J.F. and F.R. Furuya 1991 Gold Nanoparticles for Radiation Enhancement in Vivo. *J Histochem Cytochem.* **40**(2) 177-184.
11. Chattopadhyay, N., et al. 2013 Molecularly targeted gold nanoparticles enhance the radiation response of breast cancer cells and tumor xenografts to X-radiation. *Breast Cancer Res Treat.* **137**(1) 81-91.
12. Nie, S. 2010 Understanding and overcoming major barriers in cancer nanomedicine. *Nanomedicine (Lond).* **5**(4) 523-8.
13. Dixit, V., et al. 2006 Synthesis and grafting of thioctic acid-PEG-folate conjugates onto Au nanoparticles for selective targeting of folate receptor-positive tumor cells. *Bioconjug Chem.* **17**(3) 603-9.
14. Haller, E., W. Lindner, and M. Lammerhofer 2015 Gold nanoparticle-antibody conjugates for specific extraction and subsequent analysis by liquid chromatography-tandem mass spectrometry of malondialdehyde-modified low density lipoprotein as biomarker for cardiovascular risk. *Anal Chim Acta.* **857** 53-63.

15. Patra, C.R., et al. 2008 Targeted delivery of gemcitabine to pancreatic adenocarcinoma using cetuximab as a targeting agent. *Cancer Res.* **68**(6) 1970-8.
16. Montenegro, J.M., et al. 2013 Controlled antibody/(bio-) conjugation of inorganic nanoparticles for targeted delivery. *Adv Drug Deliv Rev.* **65**(5) 677-88.
17. Jiang, W., et al. 2008 Nanoparticle-mediated cellular response is size-dependent. *Nat Nanotechnol.* **3**(3) 145-50.
18. Bhattacharyya, S., et al. 2010 Nanoconjugation modulates the trafficking and mechanism of antibody induced receptor endocytosis. *Proc Natl Acad Sci U S A.* **107**(33) 14541-6.
19. Brust, M., et al. 1994 Synthesis of thiol-derivatised gold nanoparticles in a two-phase Liquid–Liquid system. *J. Chem. Soc., Chem. Commun.* **0**(7) 801-802.
20. Ackerson, C.J., et al. 2010 Synthesis and bioconjugation of 2 and 3 nm-diameter gold nanoparticles. *Bioconjug Chem.* **21**(2) 214-8.
21. Levi-Kalisman, Y., et al. 2011 Synthesis and Characterization of Au102(p-MBA)44 Nanoparticles. *J Am Chem Soc.* **133**(9) 2976-2982.
22. Marjomaki, V., et al. 2014 Site-specific targeting of enterovirus capsid by functionalized monodisperse gold nanoclusters. *Proc Natl Acad Sci U S A.* **111**(4) 1277-81.
23. Desplancq, D., et al. 2018 Cytosolic Diffusion and Peptide-Assisted Nuclear Shuttling of Peptide-Substituted Circa 102 Gold Atom Nanoclusters in Living Cells. *ACS Applied Nano Materials.* **1**(8) 4236-4246.
24. Yao, H., et al. 2016 Methods to Design and Synthesize Antibody-Drug Conjugates (ADCs). *Int J Mol Sci.* **17**(2).
25. Billah, M.M., et al. 2010 Directed immobilization of reduced antibody fragments onto a novel SAM on gold for myoglobin impedance immunosensing. *Bioelectrochemistry.* **80**(1) 49-54.
26. Ackerson, C.J., R.D. Powell, and J.F. Hainfeld 2010 Site-Specific Biomolecule Labeling with Gold Clusters. *Methods Enzymol.* **481** 195-230.
27. Diebolder, C.A., et al. 2014 Complement is activated by IgG hexamers assembled at the cell surface. *Science.* **343**(6176) 1260-3.
28. He, W., et al. 2007 A freeze substitution fixation-based gold enlarging technique for EM studies of endocytosed Nanogold-labeled molecules. *J Struct Biol.* **160**(1) 103-13.
29. Lévy, R., et al. 2004 Rational and Combinatorial Design of Peptide Capping Ligands for Gold Nanoparticles. *J Am Chem Soc.* **126**(32) 10076-10084.
30. Laemmli, U.K. 1970 Cleavage of Structural Proteins during the Assembly of the Head of Bacteriophage T4. *Nature.* **227** 680.
31. Bonavia, R., et al. 2012 EGFRvIII promotes glioma angiogenesis and growth through the NF-kappaB, interleukin-8 pathway. *Oncogene.* **31**(36) 4054-66.
32. Chiper, M., et al. 2017 Self-aggregating 1.8kDa polyethylenimines with dissolution switch at endosomal acidic pH are delivery carriers for plasmid DNA, mRNA, siRNA and exon-skipping oligonucleotides. *J Control Release.* **246** 60-70.
33. Pinel, S., et al. 2014 Quantitative measurement of delivery and gene silencing activities of siRNA polyplexes containing pyridylthiourea-grafted polyethylenimines. *J Control Release.* **182** 1-12.
34. Fraser-Pitt, D.J., et al. 2011 Phosphorylation of the epidermal growth factor receptor (EGFR) is essential for interleukin-8 release from intestinal epithelial cells in response to challenge with Escherichia coli O157 : H7 flagellin. *Microbiology.* **157**(Pt 8) 2339-47.

35. Danscher, G. and J.O.R. Nörgaard 1983 Light microscopic visuaization of colloidal gold on resin-embedded tissue. *J Histochem Cytochem.* **31**(12) 1394-1398.
36. Wong, O.A., W.S. Compel, and C.J. Ackerson 2015 Combinatorial Discovery of Cosolvent Systems for Production of Narrow Dispersion Thiolate-Protected Gold Nanoparticles. *ACS Combinatorial Science.* **17**(1) 11-18.
37. Amendola, V. and M. Meneghetti 2009 Size Evaluation of Gold Nanoparticles by UV−vis Spectroscopy. *J Phys Chem C.* **113**(11) 4277-4285.
38. Makaraviciute, A., et al. 2016 Considerations in producing preferentially reduced half-antibody fragments. *J Immunol Methods.* **429** 50-6.
39. Desplancq, D., et al. 2016 Targeting the replisome with transduced monoclonal antibodies triggers lethal DNA replication stress in cancer cells. *Exp Cell Res.* **342**(2) 145-58.
40. Okada, Y., et al. 2017 EGFR Downregulation after Anti-EGFR Therapy Predicts the Antitumor Effect in Colorectal Cancer. *Mol Cancer Res.* **15**(10) 1445-1454.
41. Sorkin, A. and J.E. Duex 2010 Quantitative analysis of endocytosis and turnover of epidermal growth factor (EGF) and EGF receptor. *Curr Protoc Cell Biol.* **Chapter 15** Unit 15 14.
42. Brand, T.M., M. Iida, and D.L. Wheeler 2011 Molecular mechanisms of resistance to the EGFR monoclonal antibody cetuximab. *Cancer Biol Ther.* **11**(9) 777-792.
43. Bowman, M.C., et al. 2008 Inhibition of HIV fusion with multivalent gold nanoparticles. *J Am Chem Soc.* **130**(22) 6896-7.
44. Hainfeld, J.F., et al. 2013 Gold nanoparticle imaging and radiotherapy of brain tumors in mice. *Nanomedicine (Lond).* **8**(10) 1601-9.
45. Polyakov, A., et al. 2018 Gold Decoration and Photoresistive Response to Nitrogen Dioxide of WS2 Nanotubes. *Chemistry.*
46. Choi, B.J., et al. 2018 A gold nanoparticle system for the enhancement of radiotherapy and simultaneous monitoring of reactive-oxygen-species formation. *Nanotechnology.* **29**(50) 504001.
47. Cole, L.E., et al. 2018 Effects of Bisphosphonate Ligands and PEGylation on Targeted Delivery of Gold Nanoparticles for Contrast-Enhanced Radiographic Detection of Breast Microcalcifications. *Acta Biomaterials.* **82** 122-132.
48. Mahmoodzadeh, F., et al. 2018 A novel gold-based stimuli-responsive theranostic nanomedicine for chemo-photothermal therapy of solid tumors. *Mater Sci Eng C Mater Biol Appl.* **93** 880-889.
49. Chattopadhyay, N., et al. 2010 Design and characterization of HER-2-targeted gold nanoparticles for enhanced X-radiation treatment of locally advanced breast cancer. *Mol Pharm.* **7**(6) 2194-206.
50. Qian, Y., et al. 2014 Enhanced cytotoxic activity of cetuximab in EGFR-positive lung cancer by conjugating with gold nanoparticles. *Sci Rep.* **4** 7490.
51. Monopoli, M.P., et al. 2012 Biomolecular coronas provide the biological identity of nanosized materials. *Nat Nanotechnol.* **7**(12) 779-86.
52. Walkey, C.D., et al. 2014 Protein corona fingerprinting predicts the cellular interaction of gold and silver nanoparticles. *ACS Nano.* **8**(3) 2439-55.
53. Perrault, S.D., et al. 2009 Mediating tumor targeting efficiency of nanoparticles through design. *Nano Lett.* **9**(5) 1909-15.
54. Wong, O.A., et al. 2013 Structure-activity relationships for biodistribution, pharmacokinetics, and excretion of atomically precise nanoclusters in a murine model. *Nanoscale.* **5**(21) 10525-33.

55. Choi, H.S., et al. 2007 Renal clearance of quantum dots. *Nat Biotechnol.* **25**(10) 1165-70.
56. Shah, N.B., et al. 2012 Blood-nanoparticle interactions and in vivo biodistribution: impact of surface PEG and ligand properties. *Mol Pharm.* **9**(8) 2146-55.
57. Storm, G., et al. 1995 Surface modification of nanoparticles to oppose uptake by the mononuclear phagocyte system. *Adv Drug Deliv Rev.* **17**(1) 31-48.
58. Morais, T., et al. 2012 Effect of surface coating on the biodistribution profile of gold nanoparticles in the rat. *Eur J Pharm Biopharm.* **80**(1) 185-93.
59. Jadzinsky, P.D., et al. 2007 Structure of a thiol monolayer-protected gold nanoparticle at 1.1 A resolution. *Science.* **318**(5849) 430-3.
60. Piella, J., N.G. Bastus, and V. Puntes 2017 Size-Dependent Protein-Nanoparticle Interactions in Citrate-Stabilized Gold Nanoparticles: The Emergence of the Protein Corona. *Bioconjug Chem.* **28**(1) 88-97.
61. Saha, K., et al. 2016 Regulation of Macrophage Recognition through the Interplay of Nanoparticle Surface Functionality and Protein Corona. *ACS Nano.* **10**(4) 4421-30.
62. Al-Jawad, S.M.H., et al. 2018 Synthesis and characterization of small-sized gold nanoparticles coated by bovine serum albumin (BSA) for cancer photothermal therapy. *Photodiagnosis Photodyn Ther.* **21** 201-210.
63. Westphal, M., C.L. Maire, and K. Lamszus 2017 EGFR as a Target for Glioblastoma Treatment: An Unfulfilled Promise. *CNS Drugs.* **31**(9) 723-735.
64. Hatanpaa, K.J., et al. 2010 Epidermal Growth Factor Receptor in Glioma: Signal Transduction, Neuropathology, Imaging, and Radioresistance. *Neoplasia.* **12**(9) 675-684.
65. Zhu, J.J. and E.T. Wong 2013 Personalized medicine for glioblastoma: current challenges and future opportunities. *Curr Mol Med.* **13**(3) 358-67.
66. Kaluzova, M., et al. 2015 Targeted therapy of glioblastoma stem-like cells and tumor non-stem cells using cetuximab-conjugated iron-oxide nanoparticles. *Oncotarget.* **6**(11) 8788-8806.
67. Hainfeld, J.F., et al. 2008 Radiotherapy enhancement with gold nanoparticles. *J Pharm Pharmacol.* **60**(8) 977-85.
68. Her, S., D.A. Jaffray, and C. Allen 2017 Gold nanoparticles for applications in cancer radiotherapy: Mechanisms and recent advancements. *Adv Drug Deliv Rev.* **109** 84-101.
69. Vigderman, L. and E.R. Zubarev 2013 Therapeutic platforms based on gold nanoparticles and their covalent conjugates with drug molecules. *Adv Drug Deliv Rev.* **65**(5) 663-76.
70. Chanda, N., et al. 2010 Radioactive gold nanoparticles in cancer therapy: therapeutic efficacy studies of GA-198AuNP nanoconstruct in prostate tumor-bearing mice. *Nanomedicine.* **6**(2) 201-9.
71. Shukla, R., et al. 2012 Laminin receptor specific therapeutic gold nanoparticles (198AuNP-EGCg) show efficacy in treating prostate cancer. *Proc Natl Acad Sci U S A.* **109**(31) 12426-31.
72. Ryman, J.T. and B. Meibohm 2017 Pharmacokinetics of Monoclonal Antibodies. *CPT Pharmacometrics Syst Pharmacol.* **6**(9) 576-588.
73. Longmire, M., P.L. Choyke, and H. Kobayashi 2008 Clearance properties of nano-sized particles and molecules as imaging agents: considerations and caveats. *Nanomedicine (Lond).* **3**(5) 703-17.

74. Rovais, M.R.A., et al. 2018 Internalization capabilities of gold-198 nanoparticles: Comparative evaluation of effects of chitosan agent on cellular uptake into MCF-7. *Appl Radiat Isot.* **142** 85-91.

Supporting Information

Synthesis and biological evaluation of 2.4 nm thiolate-protected gold nanoparticles conjugated to Cetuximab for targeting glioblastoma cancer cells *via* the EGFR.

Nadja Groysbeck,[1] Audrey Stoessel,[1] Mariel Donzeau,[1] Elisabete Cruz da Silva,[2] Maxime Lehmann[2], Jean-Marc Strub,[3] Sarah Cianferani,[3] Kassiogé Dembélé,[4] Guy Zuber[1]

1. Université de Strasbourg - CNRS, UMR 7242, Laboratoire de Biotechnologie et Signalisation Cellulaire, Boulevard Sébastien Brant, F-67400 Illkirch
2. Université de Strasbourg – CNRS, UMR 7021, Laboratoire de Bioimagerie et Pathologies, Faculté de Pharmacie F-67401 Illkirch
3. Université de Strasbourg - CNRS, IPHC UMR 7178, Laboratoire de Spectrométrie de Masse BioOrganique, F-67000 Strasbourg
4. Université de Strasbourg - Institut de Physique et Chimie des Matériaux de Strasbourg (IPCMS) 23 rue du Loess, F-67034 Strasbourg

E-mail: zuber@unistra.fr

Complement to Materials and Methods

MTT assay

Cells were seeded in 96-well plates and let to adhere overnight. Antibodies, AuNP-IgG conjugates and gold nanoparticle samples were added to the cells at a concentration of 167 nM and the cells were incubated for 24h at 37°C. Thiazolyl blue tetrazolium bromide was added into each well at a final concentration of 0.5 mg/mL and cells were put at 37°C for 4h. Next the medium was removed, the formazan crystals were dissolved in DMSO and the absorbance at 570 nm was measured. The assay was performed in quintuplicates.

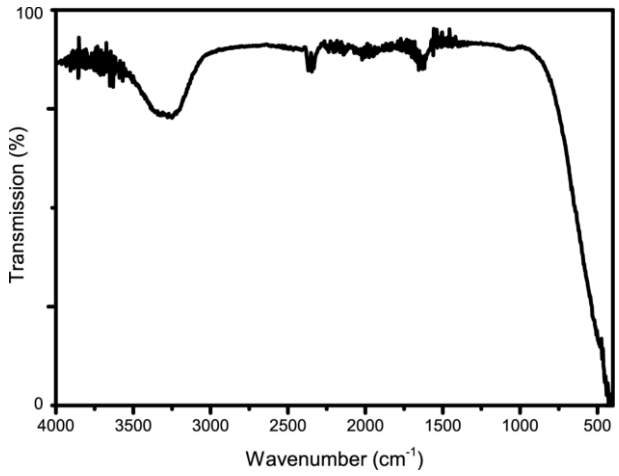

Figure S1. FTIR spectrum of 2.4 nm gold nanoparticle AuG.

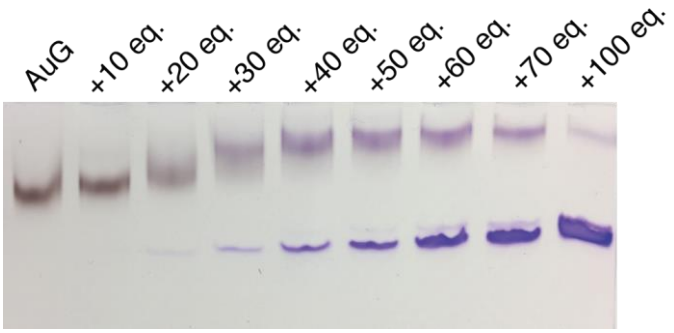

Figure S2. Functionalization of AuG with NLS (nuclear localization sequence) peptides to test how many peptides can be linked to the AuNP surface. The addition of more than 40 molar equivalents of NLS peptide to AuG did not lead to a further size increase and the amount of unreacted NLS peptide (band with higher electrophoretic mobility) increased, indicating the saturation of the AuNP surface.

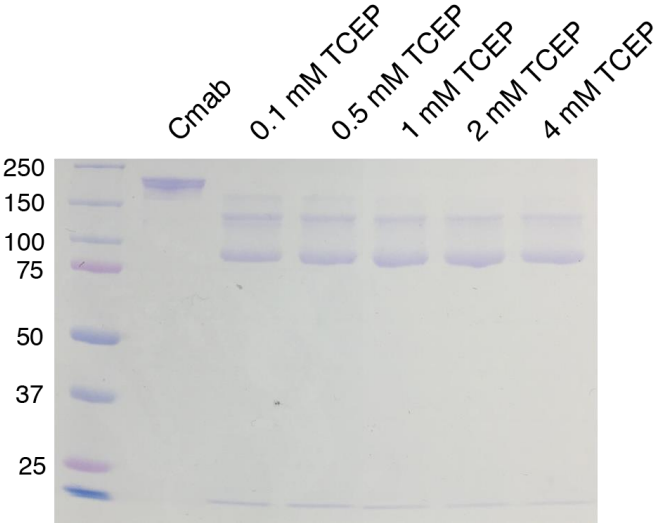

Figure S3. Evaluation of optimal TCEP (tris(2-carboxyethyl)phosphine) concentration for the reduction of Cetuximab in the hinge area. Cetuximab was incubated with increasing concentrations of TCEP and the produced reduction products were analyzed by SDS-PAGE. A TCEP concentration of 2 mM was necessary to fully reduce Cetuximab to its half antibody fragments.

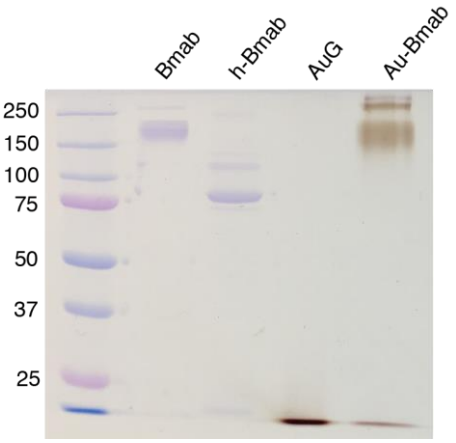

Figure S4. SDS-PAGE of gold nanoparticle-antibody-conjugate (Au-Bmab) formation under non-reducing conditions. Order on the gel from left to right: Bevacizumab (Bmab), selectively reduced Bevacizumab (h-Bmab), gold nanoparticle AuG, AuNP-Bevacizumab conjugate after passivation with peptide CALNNG (Au-Bmab)

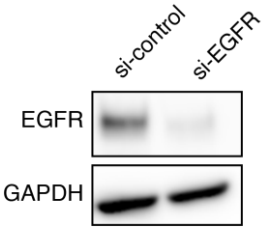

Figure S5. Evaluation of EGFR protein levels by western blot after 48h transfection with siRNA against EGFR. GAPDH was used as loading control.

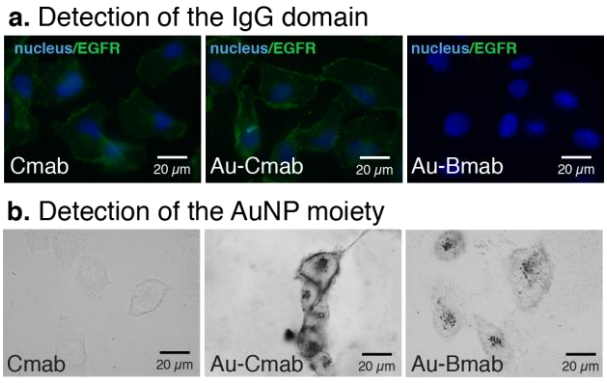

Figure S6. Evaluation of the EGFR binding ability of the anti-EGFR Cmab, Au-Cmab and Au-Bmab to living HT-1080 human fibrosarcoma cells. **(a)** Detection of the antibody domain of the nanomaterial by immunofluorescence; **(b)** Detection of the AuNP domain by silver staining. Cells were incubated with 167 nM of antibody or AuNP-antibody conjugate for 30 min at 37°C. Scale bar: 20 µm

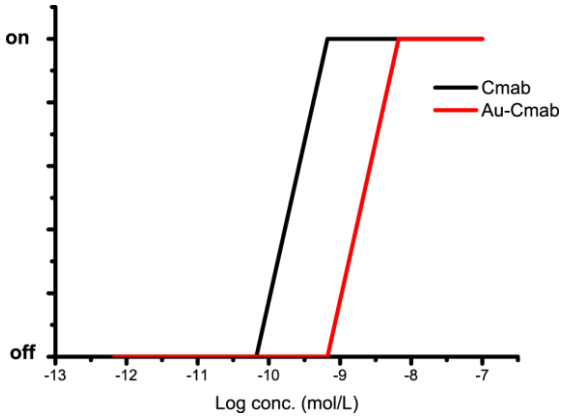

Figure S7. Quantitative analysis of the ability of Cmab and Au-Cmab to detect EGFR onto living EGFR(+) U87 cells. Increased concentrations of Cmab and Au-Cmab were added to the cells and the binding of the antibody was measured by immunofluorescence. Detection (on) or non-detection (off) of fluorescence was plotted as a function of the Cmab and Au-Cmab concentrations. Cells were incubated at 37°C for 30 min.

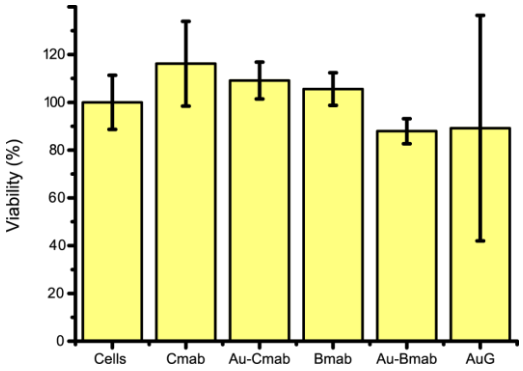

Figure S8. MTT cell viability assay using the EGFR(+) U87 cell line. Cells were incubated with Cmab, Au-Cmab, Bmab, Au-Bmab and AuG for 24h at 37°C, using a concentration of 167 nM, before addition of thiazolyl blue tetrazolium bromide. Cells incubated with medium served as a control, representing 100% viability. Values indicate the averages and standard deviations of quintuplicates.